Cuboidal supraparticles self-assembled from cubic CsPbBr3 perovskite nanocrystals

THE JOURNAL OF PHYSICAL CHEMISTRY C

Subscriber access provided by UNIVERSITY OF TOLEDO LIBRARIES

C: Physical Processes in Nanomaterials and Nanostructures

Cuboidal Supraparticles Self-Assembled from Cubic CsPbBr Perovskite Nanocrystals

Julia S. Van Der Burgt, Jaco J. Geuchies, Berend Van Der Meer, Hans Vanrompay, Daniele Zanaga, Yang Zhang, Wiebke Albrecht, Andrei V Petukhov, Laura Filion, Sara Bals, Ingmar Swart, and Daniël Vanmaekelbergh

J. Phys. Chem. C, **Just Accepted Manuscript** • DOI: 10.1021/acs.jpcc.8b02699 • Publication Date (Web): 14 Jun 2018

ACS Publications

is published by the American Chemical Society. 1155 Sixteenth Street N.W., Washington, DC 20036

Cuboidal Supraparticles Self-Assembled from Cubic $CsPbBr_3$ Perovskite Nanocrystals

Julia S. van der Burgt[1], Jaco J. Geuchies[1*], Berend van der Meer[2], Hans Vanrompay[3], Daniele Zanaga[3], Yang Zhang[3], Wiebke Albrecht[2], Andrei V. Petukhov[4,5], Laura Filion[2], Sara Bals[3], Ingmar Swart[1], Daniël Vanmaekelbergh[1]*

1. Condensed Matter and Interfaces, Debye Institute for Nanomaterials Science, Utrecht University

2. Soft Condensed Matter, Debye Institute for Nanomaterials Science, Utrecht University

3. Electron Microscopy for Materials Science, University of Antwerp

4. Physical and Colloidal Chemistry, Debye Institute for Nanomaterials Science, Utrecht University

5. Laboratory of Physical Chemistry, Department of Chemical Engineering and Chemistry, Eindhoven University of Technology

*These authors contributed equally

KEYWORDS (Word Style "BG_Keywords"). Perovskite nanocrystals, self-assembly, electron tomography, vacancies, Monte Carlo simulations.

ABSTRACT (Word Style "BD_Abstract"). Colloidal $CsPbBr_3$ nanocrystals (NCs) have emerged as promising candidates for various opto-electronic applications, such as light emitting diodes, photodetectors and solar cells. Here, we report on the self-assembly of cubic NCs from an organic suspension into ordered cuboidal supraparticles, and their structural and optical properties. Upon increasing the NC concentration or by addition of a non-solvent, the formation of the supraparticles occurs homogeneously in the suspension, as monitored by in-situ X-ray scattering measurements. The 3-D structure of the supraparticles was resolved through HAADF-STEM and electron tomography. The NCs are atomically aligned, but not connected. We characterize NC vacancies on superlattice positions both in the bulk and on the surface of the supraparticles. The occurrence of localized atomic-type NC vacancies - instead of delocalized ones - indicates that NC-NC attractions are important in the assembly, as we verify with MC simulations. Even when assembled in supra-particles, the NCs show a bright emission, with a redshift of about 30 meV compared to NCs in suspension.

Over the past decade a large amount of research has been devoted to the properties and improvement of hybrid organic-inorganic perovskite materials (e.g. $CH_3NH_3PbX_3$, X = Cl, Br, I) for solar cell applications[1], which has led to an increase in efficiency from 3.8%[2] to over 20%[3]. This success has motivated researchers all over the world to study other types of perovskite materials and extend their optoelectronic applications to photodetectors[4,5], light emitting diodes[6–8] and one-[9] and two-photon[10] pumped gain media for lasers. Recently, cesium lead halide ($CsPbX_3$) perovskite nanocrystals (NCs) have been reported as a new and promising branch of perovskites. These colloidal NCs can be synthesized with a facile hot-injection method and possess a bright emission and readily tunable opto-electronic properties[11]. In comparison to the hybrid $CH_3NH_3PbX_3$ compounds, the all-inorganic $CsPbX_3$ have a better temperature stability [5]. Moreover these NCs show narrow emission peaks with a FWHM of 50-80 meV and exhibit quantum yields of up to 90% without any extra passivation of the NC surface[12]. The emission can be tuned over the full visible spectrum by varying the composition of the X-anionic sublattice, either directly or by post-synthetic anion exchange reactions[13–15].

NCs with a low polydispersity and high photoluminescence quantum yields are ideal building blocks for larger structures with pre-designed opto-electronic functionalities. In these superlattices, new properties can arise from the electronic and/or magnetic coupling between constituent NCs. For example, the new functionality that arises from ordered structures of NCs has been used already in magnetic devices[16] and for electronic applications[17]. Here, we report on the self-assembly of cubic-shaped $CsPbBr_3$ NCs into cuboidal supraparticles (SPs), each SP consisting of several hundreds to thousands of NCs. Using in-situ X-ray scattering measurements we show that the SPs nucleate and grow in the solution upon increasing NC concentration or by addition of a non-solvent. The structure of the superlattices has been studied with (scanning) transmission

electron microscopy ((S)TEM), electron diffraction (ED) and high-angle annular dark-field (HAADF) STEM tomography. We show that the NCs form a simple cubic lattice, and are atomically aligned but not connected. We observed empty superlattice positions, i.e. vacancies similar to those in an atomic crystal, in the bulk as well as on surface lattice positions. Vacancies positioned at lattice sites should be distinguished from delocalized vacancies predicted for the hard cube model[18]. Our results thus indicate that attractive interactions between the constituent NCs are important in the self-assembly process. We studied the photoluminescence of individual SPs with confocal micro-spectroscopy. Despite the fact that exciton energy transfer can occur, the SPs still show a bright photoluminescence, red-shifted by 30 meV compared to a diluted NC solution.

RESULTS AND DISCUSSION

Formation of cuboidal supraparticles. In general, two methods can be used to induce aggregation of NCs in solution: (1) solvent evaporation, also shown by Kovalenko et al.[19], which increases the NC concentration, and (2) by addition of anti-solvent increasing the potential energy per nanocrystal. We used methyl acetate as an anti-solvent since it is one of the few polar solvents that does not damage the NCs[20]. The use of other polar media, such as methanol, ethanol, acetone and acetonitrile as an anti-solvent all lead to dissolution of the individual NCs. Both methods give identical supraparticles, however larger supraparticle sizes are obtained by solvent evaporation (see SI, Figure S4). The drawback of solvent evaporation is that the supraparticle formation takes rather long (> 1 month at room temperature). When we consider self-assembly in a reasonable lab-time period of hours, care has to be taken to operate the assembly under nearly reversible conditions, as fast kinetics can lead to disordered, non-equilibrium structures. Indeed, we observed large clusters with an irregular shape and disordered on the NC length scale, when a relatively high

amount of anti-solvent was added (see SI, Figure S5) to speed up the supraparticle formation. The structures that we will discuss were obtained under nearly reversible conditions. A more detailed description of the parameters which were used during the self-assembly process can be found in the Supporting Information.

Figure 1 shows self-assembled NC supraparticles in a series of high-angle annular dark-field (HAADF) scanning transmission electron microscopy (STEM) images with increasing magnification. A low magnification image is presented in Figure 1(a). The supraparticles appear as large white cuboids on a dark background. At higher magnifications, it becomes clear that each supraparticle consists of several hundreds of NCs (Figures 1(b-d)). Moreover, the columns of NCs are clearly distinguished at the highest magnification image (Figure 1(d)). The degree of ordering inside the supraparticle is apparent through the observed contrast in the HAADF-STEM images, hinting towards a simple cubic stacking of the NCs inside the cuboidal supraparticle. The NCs are clearly not atomically attached as has been observed for superlattices of PbSe NCs[21], but they are still separated from each other most likely by their oleate- and oleylamine ligands. The alignment must hence be related to the dense cubic stacking of the NC building blocks. The contrast in between the particles seems to be blurred-out slightly, which we tentatively ascribe to some positional and rotational disorder of the NCs inside the supraparticle. More images of the formed supraparticles can be found in the Supporting Information (SI), Figure S3. Although cubic particles can theoretically achieve high packing fractions up to 100%, they are not often encountered in nature. In the $CsPbBr_3$ SPs discussed here, cubic symmetry emerges over three length scales: on the scale of the atomic lattice, the NC building blocks in the supra particle superlattice, and the cuboidal shape of the supraparticle itself.

To properly quantify the rotational freedom of the $CsPbBr_3$ NCs inside the supraparticles, we performed electron diffraction (ED) experiments on the supraparticle presented in Figure 1. The selected-area (SA) ED pattern is shown in Figure 2(a). The presence of well-defined diffraction spots, instead of powder rings, already indicates that the particles are (nearly) atomically aligned, with the three [001] type zone-axes directed in the principal directions of the NC superlattice (i.e. one of the NC {100} facets pointing upwards). The diffraction pattern can be indexed up to reflections from the {420} atomic planes. In Figure 2(b), azimuthal traces at constant scattering vector **q** are presented for reflections from the {100}, {110}, {200} and {220} planes (depicted in red, blue, green and yellow respectively). The 12 peaks are fitted with Gaussian functions to obtain an average full-width at half-maximum (FWHM) of 9.6 ± 1.4^{o}, which reflects an upper limit of their in-plane rotational freedom. The high degree of atomic alignment of the NCs inside the supraparticles originates from the densest possible stacking of NC building blocks with a uniform cubic shape and size.

It is also relevant to characterize the structure of the NC assemblies formed in the suspension before they were scooped and dried on a TEM grid. Therefore, we performed in-situ transmission small (wide) -angle X-ray scattering (SAXS, WAXS) measurements, on pure stable NC suspensions, and on suspensions in which NC assembly was initiated by adding methyl acetate as an anti-solvent. A schematic of the experiment is shown in Figure 3(a). A solution of NCs is added into a quartz capillary with an outer diameter of 1.5 mm and placed inside a Linkam stage, positioned at a distance of 1 m from the SAXS detector. The WAXS detector, collecting the atomic diffraction of the NCs, was positioned at the inlet of the vacuum tube holding the SAXS detector.

The SAXS and WAXS patterns of a stable suspension are shown in Figure 3(b). The SAXS region (light blue) only shows form factor scattering from dispersed NCs. The WAXS signal (dark blue) shows sharp diffraction peaks, originating from the atomic perovskite lattice of the NCs. A sample with a volume fraction of 0.2 methyl acetate was measured after three days of incubation and is presented in Figure 3(c). The SAXS pattern shows clear Bragg peaks at positions of 0.55 nm^{-1}, 0.78 nm^{-1}, 1.11 nm^{-1} and 1.23 nm^{-1}. Their relative peak positions correspond to $1 : \sqrt{2} : 2 : \sqrt{5}$, which corresponds to scattering from the {100}, {110}, {200} and {210} lattice plane of a simple cubic lattice of NCs. The measured NC-NC distance inside the SPs in suspension is determined to be 11.4 ± 0.1 nm, corresponding to NCs still separated by their oleate and oleylamine ligands. The FWHM of the {100} reflection is 0.378 nm^{-1}, which corresponds to spatial extend of the periodic order of roughly 166.3 nm. The supraparticle formation is reversible, as the constituent NCs readily re-disperse upon diluting the solution of supraparticles (see SI, Figure S6).

Recent work by Bertolotti et al. also showed that the $CsPbBr_3$ NCs have the tendency to stack in solution[22], similar to concentrated solutions of perovskite nanoplatelets[23]. They argue that the stacking direction occurs most likely in the {100} NC direction, similar to the NCs in the SPs in this work. Others have also found that these perovskite NCs readily assemble into one-dimensional chains by addition of molecular clusters[24,25] or through ligand-solvent interactions[26]. Such stacks could hence be a precursor phase in the formation of the supraparticles presented in this work. However, this remains to be verified by performing in-situ time-resolved SAXS and WAXS on the self-assembly process, which is beyond the scope of this article.

NC vacancies inside a supraparticle studied with HAADF-STEM tomography and Monte Carlo simulations. In order to study the geometric structure of the NCs inside the supraparticles in more detail, a single supraparticle was studied using HAADF-STEM tomography. A series of projection images was acquired with an angular range of -70° to 78° and a tilt increment of 2°. Orthogonal to that, a second tilt series was acquired from -76° to 76° to reduce the missing wedge of tilt angles to a missing pyramid[27]. Using this dual tilt series as an input for several mathematical reconstruction algorithms, we found that the quality of the reconstruction was greatly improved compared to the reconstruction that was obtained from just using one tilt series.

A visualization of the acquired tomogram is presented in Figure 4(a). Unfortunately, we are not able to clearly resolve all individual NC positions inside the supraparticle; the missing pyramid of tilt angles smears out the information in the z-direction of the cuboidal supraparticle. Nonetheless, the orthoslices, taken through the center of the structure, in Figure 4(b-d) show interesting features. In all three orthogonal directions, we observe empty places on lattice positions. They appear to be localized single point vacancies and vacancy clusters. From the tomogram, we are able to estimate the volume fraction of vacancies in the bulk of the supraparticle of 3.3% assuming cubic symmetry of the NC lattice (see SI for more details). Furthermore, we also performed secondary-electron (SE)-STEM to acquire information on the surface of the supraparticles, which can be found in the SI (Figures S7 and S8). Also, on the surface of the supraparticles, we observe localized NC vacancies and groups of missing NCs. We estimate that the amount of missing surface NCs roughly equals 5.5 ± 1.5%.

Interestingly, the localized nature of the NC vacancies is in contrast to previous Monte Carlo and molecular dynamics simulations for hard cubes, i.e. cubes that interact only through excluded volume interactions. Smallenburg et al. showed that for hard cubes, vacancies manifest themselves

as a finite-length chain of particles along one of the principal axes in the crystal[18]. The vacancy is thus spread over many lattice positions. More specifically, in this hard-cube system, the equilibrium concentration of vacancies is very high (up to 6%) due to the fact that creating a vacancy provides additional free volume for multiple nearby particles, which increases the entropy of the crystal. Note that in a system of attractive cubes, Rossi et al. observed localized NC vacancies, where colloidal cubes of roughly one micron are self-assembled into simple cubic lattices through addition of a depletant, which induces effective attractions between the cube facets[28]. As such we propose that the localization and grouping of NC vacancies in our experiments point towards attractive interactions between the NCs during the self-assembly. Specifically, for sufficiently large NC-NC attractions, the free energy will be minimized when the particles in the vicinity of the vacancy are sitting on regular lattice positions, as the cost of breaking cohesive bonds will dominate over the entropic gain associated with vacancy delocalization.

In order to understand the observed localization of the vacancies, we performed Monte Carlo simulations of cubes in the NVT ensemble, where N (the number of particles), V (the volume) and T (the temperature) are fixed, and the cube-cube attraction can be changed from zero to several times the thermal energy. As a minimal model that captures the repulsive core and an attraction, we model the interactions between the cubes as a combination of a cubic hard-core repulsion and a spherically-symmetric square well attraction originating from the center of the cube. The range of the attractive square well was fixed to $\Delta = 1.14\sigma$, with σ the edge length of the cubes, and we varied the well depth $\beta\varepsilon$, with $\beta = 1/k_bT$. Thus, for the $\beta\varepsilon = 0$ our model reduces to the hard cubes model with delocalized vacancies, and we can study the effect of increasing the attraction strength $\beta\varepsilon$ on the vacancy structure. While the nucleation of these supraparticles is described in the SI (Figure S12), we will now focus on the (de-)localization of defects in the bulk of the crystal. In

these simulations, we start off from a perfect simple cubic crystal at a fixed packing fraction of $\varphi = 0.80$ and initialized a single vacancy by removing a single particle. In agreement with Ref. 22 we observe NC vacancies to be delocalized over many lattice positions for the hard-cube system, $\beta\varepsilon = 0$ (Figure 5(a)). Yet, upon introducing a slight attraction between the cubes, $\beta\varepsilon = -0.5$, the long delocalized NC vacancies are not observed anymore (Figure 5(b)). Instead, the NC vacancies spread only over a couple of lattice sites. Thus, already for a moderate attraction strength between the particles, we observe the defect structure to be dominated by the cohesive bonds between the particles. For slightly larger attractions, $\beta\varepsilon = -1$, we observe the particles in the vicinity of the NC vacancies exclusively on lattice positions, and no delocalized NC vacancies are observed (Figure 5(c)), similar to the tomography experiments presented in Figure 4.

Optical properties of supraparticles compared to NCs in solution. Often, quantum-dot solids suffer from a reduced PL quantum yield, as exciton energy transfer between the nanocrystals in the solid enhances the probability of non-radiative energy transfer. We found that $CsPbBr_3$ SPs deposited on a glass slide remained strongly emissive, with a photoluminescence quantum yield of 26%, as determined with an integrating sphere. This is good news for several opto-electronic applications requiring a QD solid as the optically active material. In order to study the optical properties of individual supraparticles in more detail, we performed confocal microspectroscopy. A dispersion containing the supraparticles was drop cast on a microscope slide and the solvent of the dispersion was allowed to evaporate. A droplet of immersion oil was placed on the sample, and a second cover slide was placed on top of the sample. The results are presented in Figure 6 and in the Supporting Information, Figure S13.

Figure 6 shows the PL spectra of many spots observed on the glass slide. Fig. 6(a) shows the confocal micrograph of a glass slide covered with supraparticles. The circled areas indicate the regions where the PL signal was integrated. In Figures 6(b) we present the peak energies of 30 spots vs. the intensity and observe a gradual redshift (shown in Figure 6(c)), that abruptly becomes constant at sufficiently high spot intensity, the overall redshift being roughly 30 meV. A similar redshift is observed when the PL spectra of dispersed NCs and dispersed supraparticles are compared (SI, Figures S14 and S15). We hence conclude that the bright spots present regions of supraparticles, and the weak spots individual NCs or smaller clusters.

The redshift observed in the emission of the supraparticles with respect to individual NCs could have several causes: Bodnarchuk et al. reported in their recent work[19], that the relative increase in the dielectric constant of the NC environment can cause a redshift if the electron and hole both become more delocalized. Furthermore, the excitons in the NCs are in the weak confinement regime; the electronic coupling between NCs inside a supraparticle could thus also cause a weak redshift of the PL spectrum. Third, exciton energy transfer results in a spatial diffusion of the excitons over the superlattice, always with a trend towards lower exciton energy. Di Stasio et al. reported a similar shift of the PL in concentrated solutions of $CsPbBr_3$ NCs and solid state films[29]. This effect is also shown in concentrated solutions of the cubic $CsPbBr_3$ NCs, and is reversible upon diluting the NC dispersion[30]. In our time-resolved photoluminescence experiments (Figure S14), we observe that the shift in the PL peak position occurs faster than the time resolution of our setup (~250 ps) which is probably faster than exciton energy transfer. This indicates that energy transfer is not the cause of the observed redshift. We must conclude here that although the redshift

occurring in $CsPbBr_3$ NC supraparticles is well established, its main cause remains an outstanding question.

In summary, we have shown that $CsPbBr_3$ nanocubes self-assemble into supraparticles that have an overall cuboidal shape. In the superlattices, the nanocrystals are atomically aligned but separated by the capping ligands. Vacancies form real point defects instead of being delocalized, indicating that attractive interactions play a role in the self-assembly process. The supraparticles show a bright photoluminescence, red shifted by 30 meV with respect to that of individual NCs. The fact that the obtained supraparticles are still highly emissive makes them promising candidates for opto-electronic applications. For example, they possibly can be used as microcavities, to study the confinement of the PL and lasing inside supraparticles.

Competing financial interests

The authors declare no competing financial interests.

Corresponding author

Daniel Vanmaekelbergh: d.vanmaekelbergh@uu.nl

Acknowledgements

The authors thank Dr. Rajeev Dattani and Jacques Gorini from the ID02 beamline of the ESRF for their excellent assistance during the X-ray scattering experiments. We also thank Carlo van Overbeek, P. Tim Prins and Federico Montanarella for their support during the synchrotron experiments. The authors gratefully acknowledge Prof. dr. Alfons van Blaaderen for fruitful discussions. DV acknowledges funding from NWO-CW TOPPUNT 'Superficial superstructures'. JJG acknowledges the joint Debye and ESRF graduate programs for financial support. HV gratefully acknowledges financial support by the Flemish Fund for Scientific Research (FWO

grant 1S32617NN). SB acknowledges financial support from the European Research Council (ERC Starting Grant #335078-COLOURATOMS). YZ acknowledges financial support from the European Union's Horizon 2020 research and innovation program, under the Marie Sklodowska-Curie grant agreement #665501 through a FWO [PEGASUS]2 Marie Sklodowska-Curie fellowship (12U4917N). WA acknowledges financial support from the European Research Council under the European Unions Seventh Framework Program (FP-2007-2013)/ERC Advanced Grant Agreement 291667 HierarSACol.

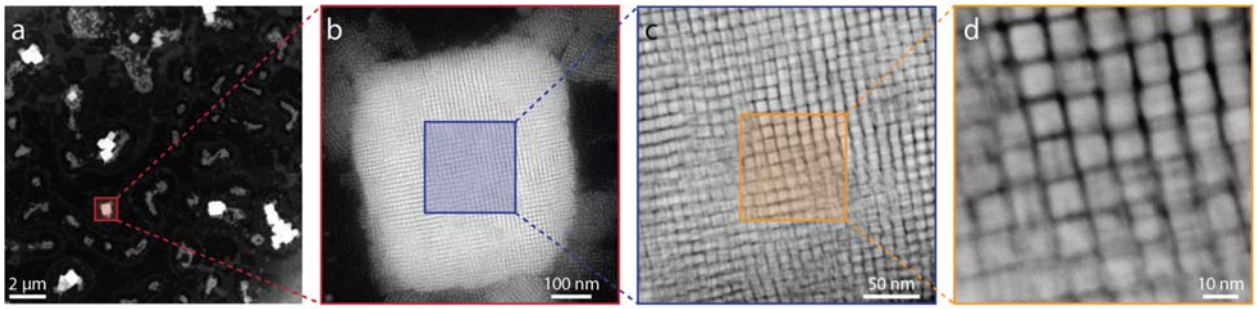

Figure 1: The structure of $CsPbBr_3$ NC supraparticles. (a) Low-magnification overview image, showing a relatively low coverage of large, cuboid-shaped supraparticles. **(b)** Zoom-in on the marked region in (a) showing a single supraparticle with a nearly cubic shape. **(c)** Zoom on the marked area in (b) showing nearly aligned nanocrystals in a dense cubic stacking**.** The individual NCs in the supraparticle are clearly visible. **(d)** Further zoom-in on the marked area in **(c)**. The columns of NCs in the lattice of the supraparticle are clearly visible, hinting towards a simple-cubic packing of the constituent NCs inside the supraparticle.

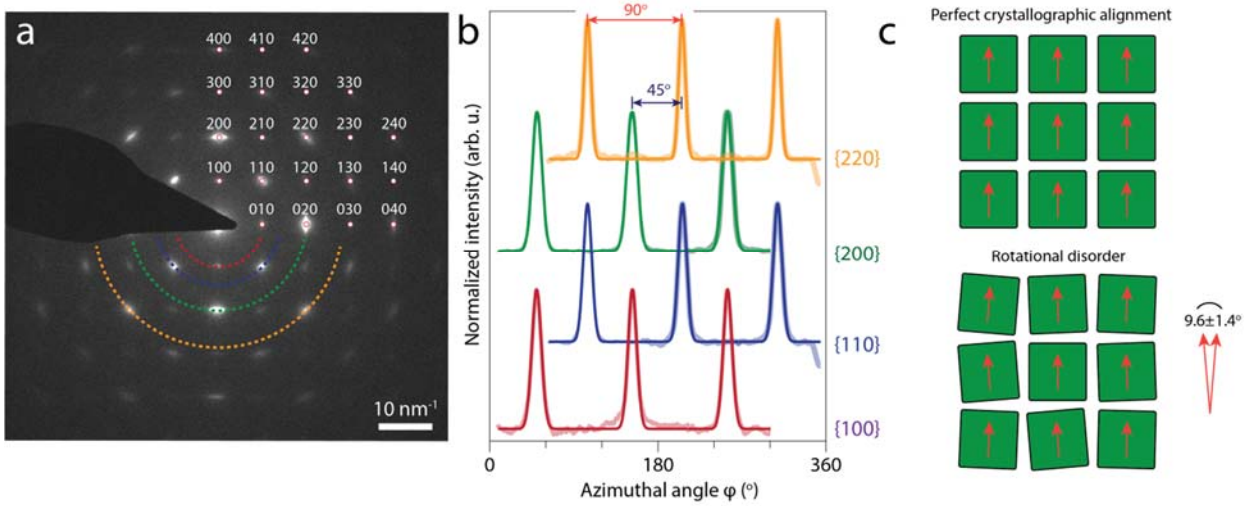

Figure 2: Electron diffraction analysis of a single supraparticle consisting of $CsPbBr_3$ NCs. **(a)** Electron diffraction pattern acquired along the [001] NC zone axis of the supraparticle shown in Figure 1. The appearance of well-defined diffraction spots indicate that the NCs are atomically aligned. The diffraction spots can be indexed clearly up to reflections from the {420} atomic planes. **(b)** Azimuthal traces at constant scattering vectors **q** for different atomic reflections, as indicated with the colored semicircles in **(a)**. Fitting the twelve peaks with Gaussian functions (solid lines) gives an average FWHM of 9.6±1.4º, which provides and upper limit of the in-plane rotational freedom of the NCs inside the supraparticle. **(c)** 2-D schemes of a planar section perpendicular to the [001] superlattice axis, demonstrating the effect of slight rotational disorder. The orange arrows represent the [100] atomic axis of each of the nanocubes.

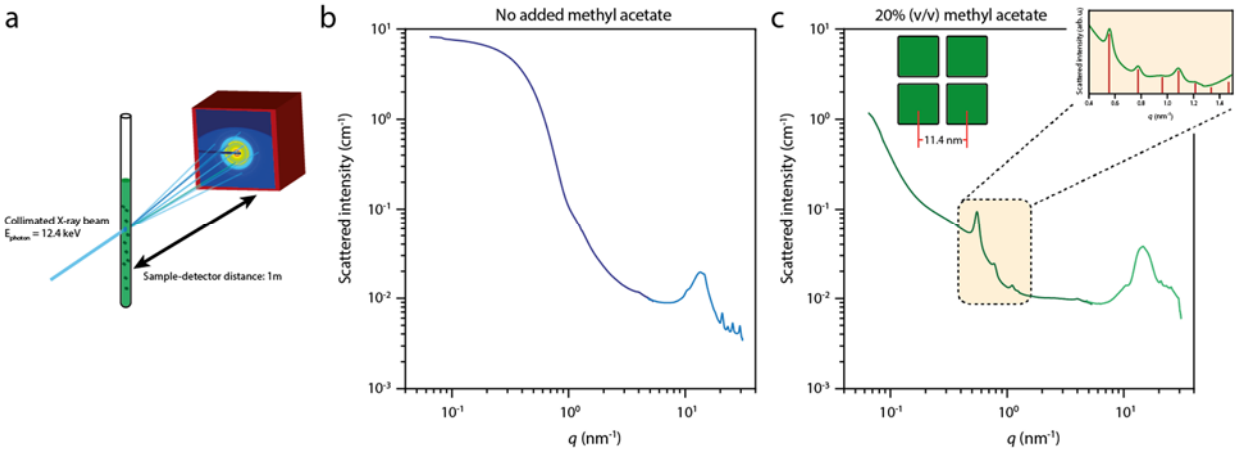

Figure 3: Transmission X-ray scattering of NC solutions during the formation of supraparticles. (a) Scheme of the experimental set-up. A quartz capillary is loaded with a solution of NCs and placed in a linkam stage, which is located 1m from the detector to collect the SAXS signal. The formation of supraparticles can be initiated by addition of an anti-solvent. **(b)** SAXS pattern of the NC dispersion without addition of anti-solvent, showing only form factor scattering of the individual NCs in solution. **(c)** SAXS pattern of the diluted NC solution after three days of incubation upon addition of 20% (v/v) of methyl-acetate anti-solvent; the Bragg reflections indicate the formation of crystalline supraparticles in the solution. The inset shows a zoom on the region with the Bragg peaks, which is scaled by the form factor scattering from **(b)**. The red lines indicate the expected peak positions for a simple-cubic packing of the NCs inside the supraparticles.

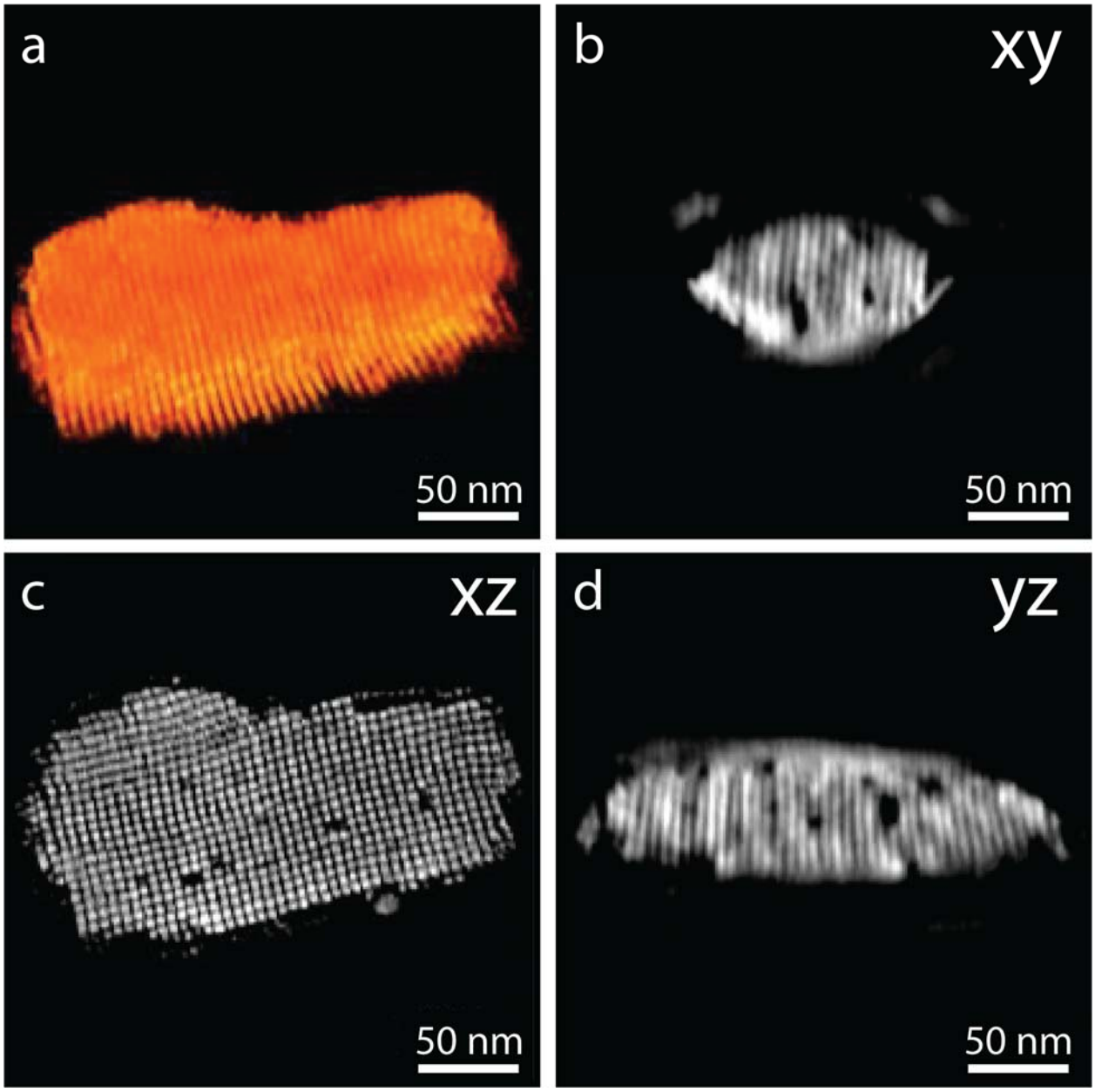

Figure 4: Lookinng inside supraparticles with HAADF-STEM tomography.
(a) Visualization of the 3-D reconstruction of a single supraparticle, acquired by rotating the sample over two orthogonal tilt series and reconstructed using a SIRT algorithm. Orthoslices through the xy **(b)**, xz **(c)** and yz **(d)** direction of the tomogram reveal several localized NC vacancies and groups of missing NCs in the bulk of the supraparticle. All vacancies are clearly defined on a lattice position.

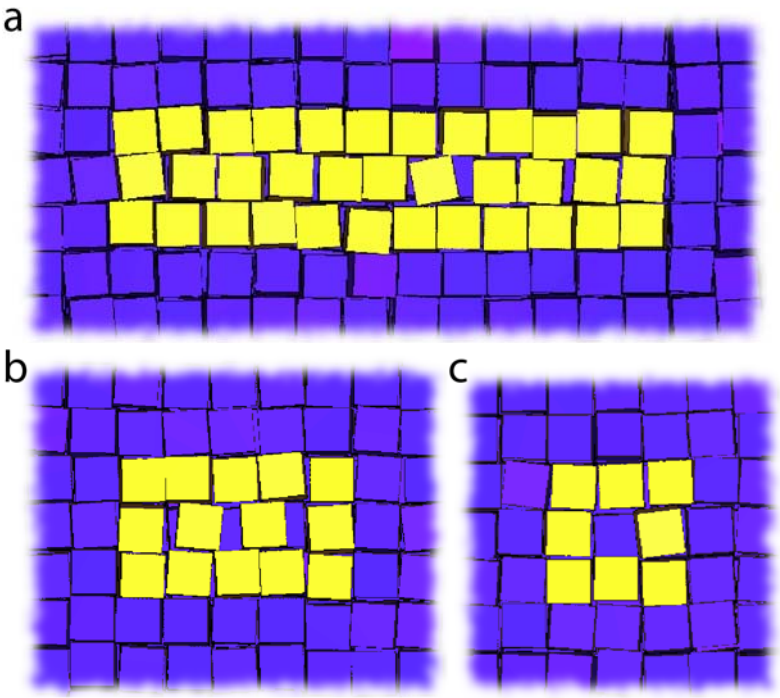

Figure 5: Monte Carlo simulations of (de-)localized NC vacancies inside the supraparticles as a function of attraction strength. (a) ε = 0 k_bT, the NC vacancy is delocalized over many lattice positions. **(b)** ε = -0.5 k_bT, long delocalized NC vacancies are not observed anymore, only weak delocalization of the NC vacancies over a maximum of a few lattice sites are observed. **(c)** ε = -1 k_bT, NC vacancies are exclusively observed on lattice positions and do not delocalize. The latter is also observed in the tomography experiments presented in Figure 4.

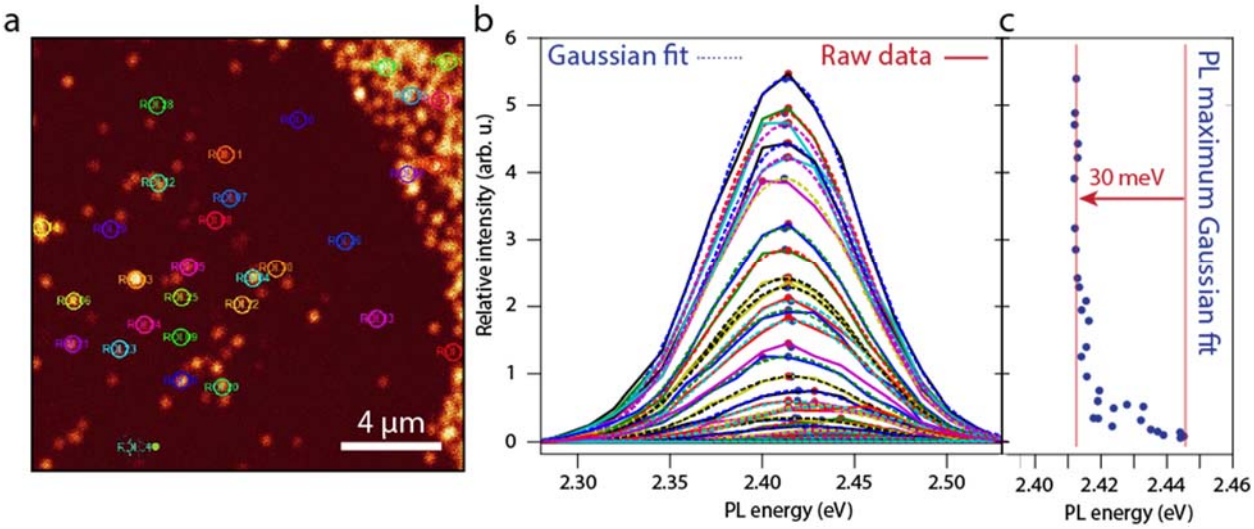

Figure 6: Confocal microspectroscopy on individual $CsPbBr_3$ NC supraparticles. (a) Confocal micrograph of a glass slide covered with supraparticles, which appear as high intensity areas on a dark background. The circles indicate the areas in which the PL signal was integrated **(b)** The PL spectra of a large number of different regions in the confocal micrograph shown in **(a)**. The solid lines indicate the raw data, whereas the dashed lines are Gaussian fits to the data. **(c)** Comparing the peak intensity to the PL energy, a redshift of roughly 30 meV is observed for the supraparticles compared to the NC monolayer background.

REFERENCES

(1) Kulbak, M.; Cahen, D.; Hodes, G. How Important Is the Organic Part of Lead Halide Perovskite Photovoltaic Cells? Efficient CsPbBr 3 Cells. *J. Phys. Chem. Lett.* **2015**, *6*, 2452–2456.

(2) Kojima, A.; Teshima, K.; Shirai, Y.; Miyasaka, T. Organometal Halide Perovskites as Visible-Light Sensitizers for Photovoltaic Cells. *J. Am. Chem. Soc.* **2009**, *131*, 6050–6051.

(3) Eperon, G. E.; Leijtens, T.; Bush, K. A.; Prasanna, R.; Green, T.; Wang, J. T.-W.; McMeekin, D. P.; Volonakis, G.; Milot, R. L.; May, R.; *et al.* Perovskite-Perovskite Tandem Photovoltaics with Optimized Bandgaps. *Science (80-.).* **2016**.

(4) Gao, J.; Nguyen, S. C.; Bronstein, N. D.; Alivisatos, A. P. Solution-Processed, High-Speed, and High-Quantum-Efficiency Quantum Dot Infrared Photodetectors. *ACS Photonics* **2016**, *3*, 1217–1222.

(5) Ramasamy, P.; Lim, D.-H.; Kim, B.; Lee, S.-H.; Lee, M.-S.; Lee, J.-S.; Manna, L.; Fiebig, M.; Heiss, W.; Kovalenko, M. V.; *et al.* All-Inorganic Cesium Lead Halide Perovskite Nanocrystals for Photodetector Applications. *Chem. Commun.* **2016**, *52*, 2067–2070.

(6) Wang, N.; Cheng, L.; Ge, R.; Zhang, S.; Miao, Y.; Zou, W.; Yi, C.; Sun, Y.; Cao, Y.; Yang, R.; *et al.* Perovskite Light-Emitting Diodes Based on Solution-Processed Self-Organized Multiple Quantum Wells. *Nat. Photonics* **2016**, *10*, 699–704.

(7) Wang, P.; Bai, X.; Sun, C.; Zhang, X.; Zhang, T.; Zhang, Y. Multicolor Fluorescent Light-Emitting Diodes Based on Cesium Lead Halide Perovskite Quantum Dots. *Appl. Phys. Lett.* **2016**, *109*, 063106.

(8) Zhang, X.; Lin, H.; Huang, H.; Reckmeier, C.; Zhang, Y.; Choy, W. C. H.; Rogach, A. L. Enhancing the Brightness of Cesium Lead Halide Perovskite Nanocrystal Based Green Light-Emitting Devices through the Interface Engineering with Perfluorinated Ionomer. *Nano Lett.* **2016**, *16*, 1415–1420.

(9) Yakunin, S.; Protesescu, L.; Krieg, F.; Bodnarchuk, M. I.; Nedelcu, G.; Humer, M.; De Luca, G.; Fiebig, M.; Heiss, W.; Kovalenko, M. V. Low-Threshold Amplified Spontaneous Emission and Lasing from Colloidal Nanocrystals of Caesium Lead Halide Perovskites. *Nat. Commun.* **2015**, *6*, 8056.

(10) Xu, Y.; Chen, Q.; Zhang, C.; Wang, R.; Wu, H.; Zhang, X.; Xing, G.; Yu, W. W.; Wang, X.; Zhang, Y.; *et al.* Two-Photon-Pumped Perovskite Semiconductor Nanocrystal Lasers. *J. Am. Chem. Soc.* **2016**, *138*, 3761–3768.

(11) Lignos, I.; Stavrakis, S.; Nedelcu, G.; Protesescu, L.; deMello, A. J.; Kovalenko, M. V. Synthesis of Cesium Lead Halide Perovskite Nanocrystals in a Droplet-Based Microfluidic Platform: Fast Parametric Space Mapping. *Nano Lett.* **2016**, *16*, 1869–1877.

(12) Protesescu, L.; Yakunin, S.; Bodnarchuk, M. I.; Krieg, F.; Caputo, R.; Hendon, C. H.; Yang, R. X.; Walsh, A.; Kovalenko, M. V. Nanocrystals of Cesium Lead Halide Perovskites (CsPbX3, X = Cl, Br, and I): Novel Optoelectronic Materials Showing Bright Emission with Wide Color Gamut. *Nano Lett.* **2015**, 1–5.

(13) Nedelcu, G.; Protesescu, L.; Yakunin, S.; Bodnarchuk, M. I.; Grotevent, M. J.; Kovalenko, M. V. Fast Anion-Exchange in Highly Luminescent Nanocrystals of Cesium Lead Halide Perovskites (CsPbX 3 , X = Cl, Br, I). *Nano Lett.* **2015**, *15*, 5635–5640.

(14) Akkerman, Q. A.; D'Innocenzo, V.; Accornero, S.; Scarpellini, A.; Petrozza, A.; Prato, M.; Manna, L. Tuning the Optical Properties of Cesium Lead Halide Perovskite Nanocrystals by Anion Exchange Reactions. *J. Am. Chem. Soc.* **2015**, *137*, 10276–10281.

(15) Koscher, B. A.; Bronstein, N. D.; Olshansky, J. H.; Bekenstein, Y.; Alivisatos, A. P.

Surface- vs Diffusion-Limited Mechanisms of Anion Exchange in $CsPbBr_3$ Nanocrystal Cubes Revealed through Kinetic Studies. *J. Am. Chem. Soc.* **2016**, jacs.6b08178.

(16) Dong, A.; Chen, J.; Vora, P. M.; Kikkawa, J. M.; Murray, C. B. Binary Nanocrystal Superlattice Membranes Self-Assembled at the Liquid-Air Interface. *Nature* **2010**, *466*, 474.

(17) Dong, A.; Jiao, Y.; Milliron, D. J. Electronically Coupled Nanocrystal Superlattice Films by in Situ Ligand Exchange at the Liquid-Air Interface. *ACS Nano* **2013**, *7*, 10978–10984.

(18) Smallenburg, F.; Filion, L.; Marechal, M.; Dijkstra, M. Vacancy-Stabilized Crystalline Order in Hard Cubes. *Proc. Natl. Acad. Sci. U. S. A.* **2012**, *109*, 17886–17890.

(19) Kovalenko, M. V.; Bodnarchuk, M. I. Lead Halide Perovskite Nanocrystals: From Discovery to Self-Assembly and Applications. *Chim. Int. J. Chem.* **2017**, *71*, 461–470.

(20) Swarnkar, A.; Marshall, A. R.; Sanehira, E. M.; Chernomordik, B. D.; Moore, D. T.; Christians, J. A.; Chakrabarti, T.; Luther, J. M. Quantum Dot–Induced Phase Stabilization of α-CsPbI3 Perovskite for High-Efficiency Photovoltaics. *Science (80-.).* **2016**, *354*.

(21) Evers, W. H.; Goris, B.; Bals, S.; Casavola, M.; de Graaf, J.; Roij, R. van; Dijkstra, M.; Vanmaekelbergh, D. Low-Dimensional Semiconductor Superlattices Formed by Geometric Control over Nanocrystal Attachment. *Nano Lett.* **2013**, *13*, 2317–2323.

(22) Bertolotti, F.; Protesescu, L.; Kovalenko, M. V.; Yakunin, S.; Cervellino, A.; Billinge, S. J. L.; Terban, M. W.; Pedersen, J. S.; Masciocchi, N.; Guagliardi, A. Coherent Nanotwins and Dynamic Disorder in Cesium Lead Halide Perovskite Nanocrystals. *ACS Nano* **2017**, acsnano.7b00017.

(23) Bekenstein, Y.; Koscher, B. A.; Eaton, S. W.; Yang, P.; Alivisatos, A. P. Highly Luminescent Colloidal Nanoplates of Perovskite Cesium Lead Halide and Their Oriented Assemblies. *J. Am. Chem. Soc.* **2015**, *137*, 16008–16011.

(24) Zhang, X.; Lv, L.; Ji, L.; Guo, G.; Liu, L.; Han, D.; Wang, B.; Tu, Y.; Hu, J.; Yang, D.; *et al.* Self-Assembly of One-Dimensional Nanocrystal Superlattice Chains Mediated by Molecular Clusters. **2016**.

(25) Zhang, X.; Lv, L.; Wu, G.; Yang, D.; Dong, A. Cluster-Mediated Assembly Enables Step-Growth Copolymerization from Binary Nanoparticle Mixtures with Rationally Designed Architectures. *Chem. Sci.* **2018**, *9*, 3986–3991.

(26) Soetan, N.; Erwin, W. R.; Tonigan, A. M.; Walker, D. G.; Bardhan, R. Solvent-Assisted Self-Assembly of $CsPbBr_3$ Perovskite Nanocrystals into One-Dimensional Superlattice. *J. Phys. Chem. C* **2017**, *121*, 18186–18194.

(27) Arslan, I.; Tong, J. R.; Midgley, P. A. Reducing the Missing Wedge: High-Resolution Dual Axis Tomography of Inorganic Materials. *Ultramicroscopy* **2006**, *106*, 994–1000.

(28) Rossi, L.; Sacanna, S.; Irvine, W. T. M.; Chaikin, P. M.; Pine, D. J.; Philipse, A. P. Cubic Crystals from Cubic Colloids. *Soft Matter* **2011**, *7*, 4139–4142.

(29) Di Stasio, F.; Imran, M.; Akkerman, Q. A.; Prato, M.; Manna, L.; Krahne, R. Reversible Concentration-Dependent Photoluminescence Quenching and Change of Emission Color in $CsPbBr_3$ Nanowires and Nanoplatelets. *J. Phys. Chem. Lett.* **2017**, *8*, 2725–2729.

(30) de Weerd, C.; Gomez, L.; Zhang, H.; Buma, W. J.; Nedelcu, G.; Kovalenko, M. V.; Gregorkiewicz, T. Energy Transfer between Inorganic Perovskite Nanocrystals. *J. Phys. Chem. C* **2016**, *120*, 13310–13315.

TOC graphic